Supporting Information

Kagan et al. 10.1073/pnas.1002825107

SI Results

Contralateral vs. Ipsilateral Saccade Response in Ventral Middle Superior Temporal and Early Visual Areas in Monkeys. The ventral middle superior temporal (MSTv) area (1–3) exhibited contralateral tuning for cue but weakly ipsilateral tuning for saccade direction, whereas the dorsal MST (MSTd) and middle temporal (MT) areas showed contralateral tuning in both intervals (Fig. S5*C*). This distinction may be related to functional differences between the two subdivisions of MST: MSTd is thought to be specialized for optic flow analysis related to self-movement perception, whereas MSTv is involved in processing the motion of discrete objects passing through the visual field (4). Alternatively, the difference in saccade tuning may be a consequence of the retinotopic organization: MSTv mainly represents the peripheral visual field, whereas the area adjacent to MSTd as defined by Nelissen et al. (2) represents the central field and was included in our delineation of MSTd. The visual stimulation accompanying saccades can differ for peripheral and parafoveal receptive fields because of different illumination conditions within and beyond the borders of stimulus display. Similar postsaccadic ipsilateral tuning also was exhibited by early visual areas V3A in the intraparietal sulcus/parieto-occipital sulcus (*ips/pos*), V2 in the *pos*, and peripheral V1/V2 in the calcarine sulcus (Fig. S4 *A* and *B*).

Variable- and Fixed-Delay Experiments in Humans and Monkeys. The main motivation for using a variable-delay task in humans was to distinguish between the time-locked cue response and ensuing delay-period activity in the slower and more sustained human blood oxygen level-dependent (BOLD) signals (as compared with faster and more transient BOLD signals in monkeys) (Fig. 5*A* and Fig. S5). The use of randomized trial durations facilitates the computation of general linear model (GLM) contrasts for different task epochs. In monkeys, this consideration was less crucial, because the apparent cue response was separated from the delay-period activity by a clear dip (BOLD "undershoot"; Fig. 2). Nevertheless, in addition to the fixed-delay (10 s) experiment in monkeys described in the main text, we also used randomized variable delays of 6, 8, 10, and 12 s, similar to the main human experiment. In both monkeys, variable-delay data reproduced the main findings of the fixed-delay experiment, but because technical issues with the scanner resulted in suboptimal data collection in the variable-delay experiment, we used data from the fixed-delay experiment for comparison with humans.

Activation of Human Cortical Areas Outside the Classical Dorsal Frontoparietal Network. The involvement of dorsal frontoparietal areas such as the superior parietal lobule (SPL) and the human frontal eye field (FEF) in essentially all oculomotor tasks is widely acknowledged, whereas the activation of several more frontal and inferior parietal/temporal areas, especially in the left hemisphere, during simple spatial-memory maintenance tasks such as memory saccade task is still debated. The situation is complicated because many imaging studies focus exclusively on a few selected regions of interest (ROIs) and do not report the full spectrum of activations or use stringent and uniform statistical thresholds across the entire brain and do not show ROI time courses. However, any binary thresholding is an arbitrary procedure, and signal-to-noise ratio (SNR)/strength of activation may vary across the brain as a consequence of uneven off-resonance susceptibility effects and inhomogeneous RF coil coverage.

In the frontal cortex, we detected robust cue, memory-delay, and saccade activation in the bilateral middle frontal gyrus and *ifs*, assigned to the human dorsal lateral prefrontal cortex (dlPFC), and in the neighboring posterior inferior frontal gyrus (pIFG) (*cf*. only right activation reported in refs. 5 and 6). As in all previous memory saccade studies, the anterior superior frontal sulcus (*sfs*) was not significantly activated, suggesting that it is not a functional analog of the monkey principal sulcus (*cf*. refs. 6 and 7).

In the inferior parietal lobule (IPL), the angular gyrus was not significantly activated in our study. The lack of activation may be caused by the need to suppress a reflexive saccade following the transient peripheral cue. The angular gyrus was found to be more active during visually guided reflexive saccades than during voluntary "endogenous" saccades (8) and may not be significantly activated in the memory-saccade task (although the saccade location is cued "exogenously" the actual saccade is initiated "endogenously" after a long delay when no "exogenous" stimulus is present). The more anterior supramarginal gyrus (SMG) in the IPL was bilaterally activated, although right SMG activation was more extensive (*cf.* only right activation reported in ref. 9). This area did not show any contralaterality. The right SMG is implicated in visual neglect and attentional orienting (10) and has been shown previously to represent both visual fields (11). More ventral regions in posterior segment of the superior temporal sulcus (*sts*)/posterior superior temporal gyrus (STG) and middle temporal gyrus (MTG), denoted "*asts*" and "*psts*," showed mostly cue and saccade responses but very little spatially specific delay activity. These areas belong to the putative temporo-parietal junction (TPJ) region (12) and have been shown to respond differentially to relevant, irrelevant, and novel spatial cues (10, 13). The event-related averaged (ERA) time courses from all ROIs of interest are summarized in Fig. S6*F*.

Finally, early visual occipital areas were analyzed only in across-subjects GLM and are shown for control and for comparison with early visual areas in monkeys (Fig. S4 *C* and *D*). These areas show mostly contralateral cue and contralateral or ipsilateral saccade responses, although some residual memory-delay activity (or perhaps a long-lasting cue effect) is evident in the ERA time courses [e.g., in the transverse occipital sulcus (*tos*); Fig. S4*E*].

Hemispheric and Visual Field Asymmetry in Humans and Monkeys. In both species the left hemisphere exhibited stronger contralateral selectivity. The hemispheric difference was modest in monkeys but was much more pronounced in humans, especially in the delay period (Fig. S2*A*). Across monkey areas that showed robust delay-period activity [the dorsal lateral intraparietal (LIPd), anterior lateral intraparietal (aLIP), ventral lateral intraparietal (LIPv), FEF, a45, dlPFC, temporo-parietal (Tpt), temporal parietal occipital (TPO), and MT areas], the left hemisphere *CS* was higher than the right hemisphere *CS* by only 28 ± 31% and 44 ± 42% (mean ± SD) for cue and delay periods, respectively, whereas in human areas this difference was 61 ± 59% and 127 ± 47%.

To quantify the hemispheric asymmetry of contralateral tuning further, we calculated the correlation between the difference in *CS* in the left and right hemispheres ($\%CS_{LH-RH} = 100(CS_{LH} - CS_{RH}) / CS_{LH}$) and the contralateral response amplitude in corresponding trial epochs across cortical areas. Strong negative correlation in monkeys (Spearman $r = -0.53$ for cue, $r = -0.8$ for delay, $P < 0.05$, $n = 21$ areas) shows that only those areas that had little cue and memory-delay activity showed spuriously large differences between left and right *CS* (Fig. S2*A*); these differences resulted from random fluctuations in time courses. (Recall that *CS* is a normalized measure that does not take into account the absolute amplitude of the responses.) In contrast, human areas showed no significant correlation between $\%CS_{change}$ and response amplitude ($r = -0.09$, $r = -0.16$, $P > 0.05$, $n = 16$ areas),

because many areas that had robust cue and memory-delay responses also exhibited considerable asymmetry between left hemisphere and right hemisphere tuning.

The inspection of BOLD response amplitudes showed that in both species most areas in the left and right hemispheres responded nearly equally if contra- and ipsilateral responses were combined (Fig. S2*B*). However, when responses were averaged across hemispheres, both species showed stronger responses to the cues and memorized targets in the right visual field than to those in the left visual field ($P < 0.001$ for all comparisons; Wilcoxon matched pairs signed rank test across areas) (Fig. S2*C*), reflecting a stronger contralaterality (and thus predominantly smaller activations for left space) in the left hemisphere. In monkey areas that showed strong memory delay (see earlier discussion), the percentage of the difference in the response amplitude between the right and left visual fields for cue and delay periods was 24 ± 32% and 47 ± 20%, respectively (for all areas: 30 ± 41%; 51 ± 48%, respectively). For human selected parietal and frontal areas (V7, intraparietal sulcus areas 1 and 2 (IPS1/2), retinotopic IPS (retIPS), precuneus (pCu), lateral inferior FEF (lFEF), medial superior FEF (mFEF), and dlPFC), the percentage of difference was 10 ± 3% and 30 ± 5%, respectively (for all areas: 11 ± 6%; 30 ± 7%, respectively).

SI Discussion

Previous Monkey Functional MRI Studies. Several groups (e.g., refs. 2, 14–24) have applied block-design functional MRI (fMRI) in alert monkeys, focusing mostly on various aspects of visual perception during passive fixation. In addition, two block-design studies compared periods of continuous fixation vs. series of visually guided saccades, yielding saccade activation maps similar to our event-related saccade maps (25, 26).

Two previously published reports (26, 27) employed a variant of event-related analysis that used closely spaced short trials and low (>2 s) temporal resolution and thus were not able to resolve the dynamics of the BOLD time courses within each trial. Consequently, only a single averaged hemodynamic response function (HRF) time course that collapsed several events related to the cognitive set-shift was presented in the study by Nakahara et al. (27); no time courses were extracted in the study by Koyama et al. (26).

Long Delay Periods in Monkey Electrophysiology. Most monkey electrophysiology studies employ relatively short (0.5–2 s) delay periods. However, Fuster and coworkers (28–30) used delays up to 18 s in the context of delayed match-to-sample visual and somatosensory tasks but not in the context of spatial memory, and with manual responses. In a seminal paper, Funahashi et al. (31) compared 1.5-, 3-, and 6-s memory delays in the memory saccade task and found no conspicuous differences between firing time courses during these periods in prefrontal cortex. To our knowledge, the longest memory period used for recordings during a delayed oculomotor task in the parietal cortex was 3 s, in the work of Chafee and Goldman-Rakic (32). In follow-up experiments we plan to record single units and local field potential activity from frontal and parietal fMRI-identified ROIs with the same long delays that we used in fMRI experiments to enable a more direct comparison of fMRI and neuronal activity time courses.

Response Amplitude and Contralaterality in Humans: Comparison with Other Studies. Two recent fMRI studies of delayed-memory saccades (6, 33) also used long- and variable-delay periods and specifically investigated spatial tuning properties of cue and delay-period activity in human subjects. Our results generally agree with previous findings, but there are some quantitative differences. According to similarly calculated *CS* indices, we found ~1.5–2 times less contralaterality in V7, IPS1, and IPS2 areas than reported in the study of Schluppeck et al (33). Similar to the data reported by Srimal and Curtis (6) (*cf.* 10% contra-ipsilateral difference), we observed only small differential activation in contralateral trials. This difference resulted in CS_{delay} ranging from 0.24 in the IPS1 to 0.16 in the IPS2 (and 0.26 in the retIPS), as compared with 0.3–0.5 in the data of Schluppeck et al. Akin to their data, V7 had the strongest contralaterality among those three *ips* areas for the cue response. In frontal areas, our data show residually more contralaterality in the mFEF, whereas Srimal and Curtis (6) report some contralateral tuning for the lFEF but not for the mFEF. Many other human fMRI studies did not observe any significant contralateral tuning (e.g., ref. 34), and topographic phase-mapping experiments show only weak contralateral biases (*cf.* ref. 35).

We considered several possibilities that can explain the quantitative difference between our results and those of Schluppeck et al. (33). Schluppeck et al. extracted time courses from preselected ROIs that already have been shown to exhibit a topographic organization, but this procedure is unlikely to be a source of the discrepancy: In their study, preselected ROIs were quite extensive and encompassed regions comparable with those in our study. Trivially, the reason for the discrepancy may lie in the substantial variability of BOLD time courses between subjects. Schluppeck et al. used only four subjects, so it is possible that these subjects happened to exhibit stronger contralaterality. (Of course, the same argument may apply to our two monkey subjects, although our preliminary data from a third monkey, monkey F, used in a similar memory saccade task, show similarly strong contralateral cue and memory-delay responses.)

Finally, for the *CS* calculation we used actual %BOLD change response amplitude (*SI Materials and Methods*), whereas Schluppeck et al. used model fit predictors. This manipulation could not have caused a contralateral bias, because the model was linear, and predictor-response transformations would not affect the ratio between contra- and ipsilateral trials. However, the usage of fit predictors vs. response amplitude values could explain the difference between estimates of cue-to-delay ratios in our study and that of Schluppeck et al. In Schluppeck et al., the delay-period activity predictor d was modeled as a constant level spanning the entire delay period, whereas cue c was modeled as the instantaneous δ-function. Because the hemodynamic transfer function acts as a "leaky integrator," the value of d required to reach an apparent level of BOLD activation similar to the cue response peak would be quite low ($d<<c$). At the moment, it is unclear whether the assumption of constant neuronal delay activity commencing immediately after the cue is justified: It is possible, for example, that with such long delays, the delay-period activity should be divided into early cue processing and late maintenance/preparation/recall stages. Therefore, we chose to use actual %BOLD change values that do not require any prior assumptions except a nonbiased initial baseline period.

A recent fMRI study by Jack and colleagues (36) examined topographic and contralateral organization of human cortical areas using a variant of a time-unresolved delayed saccade task with closely spaced trials and short delay periods and with continuous presentation of cue-specific distractors. Although the results of this study cannot differentiate between effects of cue, distractors, and forward-and-return saccades, they convincingly show that under these conditions there is very little visual topography in extraoccipital areas. Instead, discrete parietal and frontal areas show some degree of contralateral tuning, but even in most contralateral ROIs, the ipsilateral response was approximately half as strong as the contralateral response, resulting in *CS* of ~0.33 [note that the "laterality index" used by Jack at al. was calculated as $L = (R_{contra} - R_{ipsi}) / R_{contra}$; thus L of 0.5 corresponds to *CS* of 0.33 in the formulation we and Schluppeck et al. used].

Contralaterality and Topography in the Human Posterior Parietal Cortex. Despite continuous attempts to characterize the organization of the human posterior parietal cortex (PPC) in terms of spatial, effector, and task specificity and possible monkey homologies,

the functional and anatomical complexity of parietal areas is far from being resolved. Here we mention only briefly the spatial-tuning aspect of the problem. First, several groups that used time-unresolved phase-encoding experiments reported anatomically divergent results: Sereno et al. (37) found a discrete topographic region in the medial *ips*, whereas Schluppeck et al. (35) and Silver et al. (38) show two larger regions, IPS1 and IPS2, tiling the medial SPL along the *ips* from V7 dorsally and anteriorly. More recently, Swisher et al. (39) defined, in addition to IPS1/2, two more areas, IPS3/4, located in the "vicinity" of the topographic area defined by Sereno et al (37). Additionally, Jack et al. (36) showed that the most contralateral medial *ips* area, termed "MIPS," corresponds better to the area defined by Sereno et al. (37), but they do not find contralateral tuning in regions that would be termed IPS1/2. Although some differences in tasks may account for these discrepancies, the results obtained with different tasks in the same studies and laboratories usually are more consistent than results between laboratories. Other possibilities include different analyses/software, SNR (because of field strength, RF coil, and resolution), statistical power, and variability between subjects. Most importantly, these discrepancies underscore the limitations of the phase-encoding approach in extraoccipital areas, both because of the confounding of different visual, motor, and cognitive components and because of methodological issues. The latter limitation is discussed extensively by Jack et al. (36).

Interestingly, in addition to the MIPS, which corresponds roughly to the retIPS as defined by Medendorp and colleagues (40), Jack et al. (36) reported even stronger contralaterality in the anterior pCu, in agreement with our human results.

SI Materials and Methods

All surgical and animal care procedures were done in accordance with National Institutes of Health guidelines and were approved by the California Institute of Technology Animal Care and Use Committee. Human subjects gave informed consent in accordance with the California Institute of Technology Institutional Review Board guidelines.

Monkey Experimental Preparation. Two male rhesus macaques (*Macaca mulatta*) weighting 4–5 kg were implanted with MR-compatible plastic (PEEK) headposts embedded in Palacos bone cement (BioMet). The headposts were attached to the cranium with short ceramic screws (Thomas Recording), under general anesthesia. For training and scanning, monkeys sat in a specially designed vertical MR chair (Bruker), with the head rigidly attached to the chair with a plastic headholder. The convenient upright sitting position of the animals facilitated rigorous behavioral training and scanning procedures.

MR Imaging. Monkeys were scanned in a Bruker Biospec 4.7 T/60 cm vertical bore scanner equipped with a Bruker BGA38S or (in later experiments) a Siemens Allegra AC44 gradient coil using a ParaVision 3.0.2/4.0 platform running on a Linux RedHat 6 kernel. A linear transmitter-receiver birdcage volume RF coil (Bruker) allowed whole-head homogeneous coverage. The SNR ($mean_{signal}/SD_{noise}$) in echo-planar imaging (EPI) was in the range of 80–130. First- and second-order shimming of the B_0 field was performed with the FASTMAP algorithm along six projections through a 40 mm^3 volume inside the brain. Functional images were collected with a BOLD-sensitive T_2*-weighted gradient echo (GE)-EPI single-shot sequence using TR 1 s, TE 20 ms, 60° flip angle, 200–250 kHz bandwidth, 128 × 128 matrix, 12.8 cm field of view (FoV), 1 × 1 × 2 mm voxel, and 10–14 oblique (15°) continuous slices. For registrations with EPI, in-plane structural images were obtained using T1-weighted Inversion Recovery Rapid Acquisition with Relaxation Enhancement or 2D Modified Driven Equilibrium Fourier Transform (MDEFT) sequences during each session; a whole-head high-resolution (0.5/1 mm voxel) T1-weighted 3D-MDEFT or 2D MDEFT scan was obtained in a separate session.

Human subjects (four female, seven male, all right-handed, 20–35 years old) were scanned in a Siemens Trio 3T scanner with a Siemens eight-channel phased-array receiver head coil. Functional images were collected with GE-EPI sequences using TR 2 s, TE 30 ms, 90° flip angle, 64 × 64 matrix, 192 mm FoV, 3 × 3 × 3 mm voxel, and 30–32 oblique continuous slices. In the same session, high-resolution T1-weighted magnetization-prepared rapid acquisition with gradient echo structural scans (1 × 1 × 1 mm) were acquired for anatomical localization.

Stimulus Presentation, Online Behavioral Control, and Data Acquisition. Visual stimuli were presented on 800 × 600/60 Hz LCD goggles (Resonance Technology) subtending 30 × 24° of visual angle using custom OpenGL software. Eye position was monitored at 60 Hz, ~0.15° resolution, and 0.5–1° accuracy with an MR-compatible mini-IR camera (Resonance Technology/Arrington Research) and was recorded together with stimulus and timing information and digital triggers from the scanner. Online behavioral control and feedback were implemented in a LabVIEW RT platform (National Instruments). Incorrect trials were aborted; successful trials were rewarded with a 0.5–1 mL water drop (monkeys) or an accumulative monetary reward (humans). For humans, the amount of reward for a successfully completed experiment depended on the subject's performance, which was assessed online during scanning for each trial and reported to the subject after each run.

For offline analyses, eye position was calibrated to degrees of visual angle and smoothed before computation of velocity and acceleration, which were used for automatic saccade and blink detection with a custom algorithm. Human eye data recorded in the scanner required additional removal of gradient and RF pulse interference noise, done with a custom filtering algorithm. An example of a main sequence scatter plot for saccades made by a monkey in the scanner during one functional session is shown in Fig. S7*A*. We were able to detect saccades of ≥1° amplitude reliably but not smaller fixational saccades.

The cues were chosen randomly from eight (11° eccentricity) or 18 (10°–16°) locations. The spatial configuration of the targets is shown in Fig. S7*B*. Targets (T) and central fixation point (FP) were 0.37° squares. For contralaterality analysis, we sorted eight target condition trials with saccades made to targets 1, 2, and 3 as rightward and targets 5, 6, and 7 as leftward. The central fixation window radius was 3–5°, and the peripheral saccadic target window radius was 5–7°. Larger target windows were used to accommodate memory saccade end-point inaccuracy because of long delays and a systematic upward shift (41). We also allowed transient deflections (<200 ms in monkeys; <400 ms in humans) from the fixation window to accommodate blinks that were inevitable with long fixation periods (Fig. S7*C*).

Monkeys were trained in electrophysiology enclosures (TDK) in the MRI chairs on a range of oculomotor tasks, including a standard memory saccade task. After the monkeys learned the task, we gradually increased the duration of the trials until the monkeys were able to perform trials up to 35 s long with at least a 60% success rate. Long trial duration was chosen to allow measurements of BOLD activity originating from different intervals of the task, measurements that otherwise would not be possible because of temporal delay and dispersion of the hemodynamic response. Before imaging experiments, monkeys were habituated to the acoustic noise, to sound-attenuating cushions, and to confined space during training sessions inside the scanner. Video-based motion-detection systems were used to train the monkeys to minimize their body, limb, and jaw motions and to track their behavior during scanning. Trials compromised by motion were aborted and punished with a time-out during training and scanning. Inclusion of body and limb motion signals in the behavioral paradigm was a crucial improvement for obtaining stable, high-quality functional data.

During one daily session, monkeys typically completed four to six functional runs of 20 min each, resulting in a total time of up to 3–4 h in the scanner (including shimming, adjustment, and anatomical scans). Human subjects performed a single 10 min training session inside the scanner before the start of data collection, followed by an anatomical scan and then four functional runs of 15 min each, resulting in a total time of up to 1.5 h in the scanner. Altogether, 22 sessions in two monkeys (14 and 8 sessions, respectively) and 8 sessions in eight human subjects were analyzed for the main experiment, and 14 sessions in monkeys (6 and 8 sessions, respectively) and three sessions in three human subjects were analyzed for additional experiments (variable delay in monkeys and fixed delay in humans).

Functional Data Preprocessing. The first five EPI volumes were excluded from functional analyses to remove transient effects of magnetic saturation but were used for coregistration, because they provide better contrast for anatomical landmarks. Anatomical T1-weighted scans were processed in BrainVoyager QX (Brain Innovation) and MIPAV (NIH). In monkey experiments, EPI sequences for each run were preprocessed using slice time correction, linear trend removal, and a high-pass temporal filter with three cycles per 20 min run cut-off. 3D motion correction with 6 degrees of freedom was done by registering all EPI volumes to a first volume of the last functional run in the session, which always was followed by the matching (in-plane) anatomical T1-weighted scan. The in-plane anatomical scan for each separate session was coregistered to the high-resolution structural scan in the anterior commissure–posterior commissure (AC–PC) plane, and then EPI runs were aligned to the AC–PC-registered anatomical scan using rigid body transformations. Automated alignment procedures were followed by careful visual inspection and manual fine-tuning based on anatomical landmarks. Using these transformations, 3D volume time courses were computed in AC–PC space using $1 \times 1 \times 1$ mm voxel size and a 1,000 unit image intensity threshold (mean image intensity within the brain ranged from 4,000 to 6,000 units). In human experiments, we used the same preprocessing steps, except that the high-resolution anatomical scans also were transformed from AC–PC into Talairach space. Human 3D volume time courses were computed in Talairach space using a $3 \times 3 \times 3$ mm voxel size and a 100 unit image intensity threshold (mean image intensity within the brain ranged from 500 to 700 units). No additional spatial smoothing was applied to the fMRI data. The statistical contrast maps were upsampled (interpolated) to the resolution of the anatomical scan ($0.5 \times 0.5 \times 0.5$ mm in monkeys and $1 \times 1 \times 1$ mm in humans).

Detection of Artifacts Caused by Subject Motions and Selection of Functional Data. At the high magnetic 4.7 T field, and also to lesser extent at 3 T, the EPI signal is strongly affected by the subject's body, limb, and jaw motions, even when movements occur far from the imaging volume within the RF coil (i.e., the head). This effect is the consequence of the "off-resonance" effect: body, limb, and jaw and residual head movements introduce dynamic local B_0 field fluctuations, leading to strong imaging artifacts such as changes in intensity, geometric distortion, and signal mislocalization (Fig. S7*E*). These effects are especially pronounced in the GE single-shot fast EPI sequence that is very sensitive to B_0 field inhomogeneity.

To overcome these difficulties in alert monkey experiments, we developed a technique that combined careful monitoring of body, limb, and jaw motions, rigorous training that encouraged monkeys to minimize these motions, and data selection and postprocessing analysis that used information about these parameters. During training and scanning, monkeys were monitored with IR-sensitive video cameras (standard security surveillance cameras for training in the rig and a miniature MR-compatible CMOS camera inside the scanner). The video feed was directed to a Pelco MD 2001 automatic motion-detection system which allows adjustment of the motion sensitivity threshold for a digital binary output. This signal was fed into a LabVIEW-based real-time behavioral control system as one of the behavioral parameters. The successful completion of the trial and subsequent reward delivery was contingent not only on performance of the required oculomotor task but also on the absence of body and limb motions during the entire trial. Any time a noticeable motion occurred, the trial was aborted without reward, auditory and visual behavioral feedback was delivered, and the monkey was punished with a 5- to 10-s timeout. Monkeys were trained to sit still during the entire EPI run (20 min) but were allowed to move in interrun intervals (when no gradient noise was present), which typically lasted 1–3 min. The combined information about the change of the raw EPI signal intensity, motion detection triggers, and motion correction parameters was used to extract data from epochs that were not contaminated by body and limb movements (84% of trials in monkeys and 87% of trials in humans were retained) (Fig. S7*E*). Selection of stable epochs improved the resulting ERA time courses.

Data Analysis. Data were analyzed in BrainVoyager QX and MATLAB running on a Fedora Core 5 (64 bit) Linux. All trial events—cue, direct/memory delay, saccade, target fixation, and reward delivery—were extracted and used as predictors for the GLM after convolution with the HRF (Fig. S7*D*). Events from all trials (successful and failed) were modeled to account for the overall variance. Large fixational saccades and blinks were detected also but were not used as GLM predictors for the final models, because their inclusion did not have a significant effect. In monkeys, each daily session was analyzed separately and, because principal findings were consistent across sessions, all sessions fulfilling SNR, temporal stability, and behavioral performance criteria were combined using multisession GLM. Human data were analyzed both separately using individual-subject GLM and together in across-subjects GLMs (Talairach- and cortex-based aligned).

ROIs were defined in each subject using event-related maps for contralateral +cue, +memory-delay, and +saccade contrasts, which identified voxels active during the task (6), aided by the localization to individual sulcal patterns. We also used "task epoch" right vs. left maps and (in humans) left/right relative contribution maps to highlight most contralateral clusters. The extent of ROIs for the time-course extraction was a contiguous 2.5^3 mm (15.62 mm^3) volume in monkeys and a 5^3 mm (125 mm^3) volume in humans (or less, if the span of the statistical activation map limited the amount of "significant" voxels around the ROI origin), centered on the peak of activation. The right and left homologous ROIs were defined symmetrically to the midline unless bilateral peaks of activation were clearly offset (Table S1).

For the BOLD ERA time course, only successful trials were accumulated. ERA time courses were constructed using individual baseline estimates for each single trial: mean activity in the last 3 or 4 s of the initial fixation period for monkeys and humans, respectively ("epoch-based" averaging in BrainVoyager). Following initial analyses, we applied an faster HRF for monkeys that was faster than the standard human HRF (Fig. S7*D*), because the difference in BOLD response timing was apparent in the BOLD time courses (Fig. 2*A*). This manipulation improved the resulting statistical contrast maps but has no influence on the ERA time courses, because they were calculated from the actual EPI volume data without any prior assumptions about the shape of the HRF.

To quantify ERA time courses, we estimated the mean response amplitude (A) in several intervals within the trial. For monkeys (sampling rate 1 s), the baseline interval was defined as the last 3 s of initial fixation, cue and saccade intervals were defined as 3-s intervals starting 2 s after event onset, and memory delay was defined as the last 5 s of the delay period (or the rest of the delay period for the variable-delay experiment). For humans (sampling rate 2 s,

variable-delay experiment), the baseline interval was defined as the last 4 s of initial fixation, cue and saccade intervals were defined as the 6-s intervals starting 4 s after event onset, and memory delay was defined as the last 6 s of the delay period (the shortest delay period 6 s was excluded from calculation). Mean amplitude A in these intervals for contralateral and ipsilateral trials was used to calculate the normalized CS index: $CS = (A_{contra} - A_{ipsi}) / (|A_{contra}| + |A_{ipsi}|)$ (cf. lateralization index L in ref. 33). This (nonlinear) index ranges from −1 to 1, positive values indicating contralateral tuning and negative values representing ipsilateral tuning; for example a CS 0.33 represents the case in which the contralateral amplitude is twice as large as the ipsilateral amplitude. The normalization may inflate sporadic differences when all response amplitudes in the interval are very small (e.g., in the delay period in the area that shows no significant delay activation).

ROI Definition and Nomenclature in Monkeys. Monkey ROIs were defined individually in each subject, using statistical conjunction of contralateral +cue, +memory-delay, and +saccade maps. Because the +saccade contrast always was most extensive and significant, we used it as a basis contrast effect common to all identified ROIs and added conjunction with +cue and +memory-delay effects sequentially. Maps were thresholded at a false discovery rate correction [q(FDR)] <0.05 for conjunction contrasts and q(FDR) <0.001 for individual +saccade contrast, unless noted otherwise. Thus, only areas that showed a significant saccade activation were delineated using the +saccade contrast (although these areas still might exhibit some weaker cue and memory-delay responses apparent in the time courses); other areas are based on the conjunction of [+saccade and + cue] or [+saccade and + cue and + memory delay]. The specific contrasts used for the extraction of time courses from each ROI are listed in Table S1.

We also used "task epoch" right vs. left contrasts for illustration (Fig. 2 and Figs. S3 and S4), but we did not use these contrasts for the ROI definition because this comparison was not significant in humans, and we wanted to use the same methodology in both species.

The nomenclature of monkey areas is based on the atlas of Saleem and Logothetis (42) and other references cited in the list of ROI definitions (Box S1). We used the characteristic sulcal landmarks and previously established anatomical references to delineate the ROIs in the gray matter tentatively corresponding to known areas. (This procedure was done by cross-referencing between the same high-resolution anatomical scan with and without overlaid statistical map). This anatomically aided delineation was especially important when a given contrast activation was more extensive than the 2.5 mm^3 volume used for selecting ROIs.

ROI Definition and Nomenclature in Humans. Human imaging data were analyzed in a three-step approach to ensure that we did not miss or underestimate the sites with contralateral tuning.

In the first step, we used individual subject GLM (similar to the analysis of monkey data) and overlaid statistical maps for the contralateral +cue, +memory-delay, and +saccade contrasts on the subject's anatomical scan using the same successive conjunction procedure described for monkeys in the previous section. The overlapping peaks for + cue, +memory-delay, and +saccade contrasts in loci referenced to known sulcal landmarks and/or previously reported coordinates (as detailed in Box S1) were identified as the centers of ROIs for the time-course extraction. In two of the eight subjects, the uncorrected conjunction maps were used because of the low statistical significance of cue and memory activations. The ERA time courses were extracted separately for each subject and were averaged by calculating mean of means across trials. This approach was used for the time-course results presented in the paper.

In the second step, we used across-subjects GLM for fixed-effects analysis (i.e., calculating a combined GLM across all runs and all subjects: multistudy, multisubject GLM in BrainVoyager QX) and applied the same statistical contrasts to confirm the results of the individual ROI analysis and to compare the two approaches. The resulting time courses were extracted by averaging all corresponding trials across all subjects. The results of steps 1 and 2 generally agreed, but the across-subjects GLM time courses had slightly lower amplitudes. The correspondence between steps 1 and 2 demonstrates the consistency of activations among subjects and the robustness of our individual ROI extraction procedure. This approach was used for illustration maps presented in Fig. 4, Fig. S4*C*, and Fig. S6.

In the third step, we also applied a "random effects analysis" to the across-subjects GLM calculation (RFX GLM option in BrainVoyager QX). Even though eight subjects is not a sufficient number for a proper random effects analysis, the resulting maps, although less extensive, corresponded well with the "fixed effects" GLM maps (Fig. S6*B*), further confirming that across-subjects GLM results were not biased by activations originating in only a few subjects.

Finally, we also ran the cortex-based alignment across subjects. The averaged surface reconstruction is used in Fig. 4 and Fig. S6 to display across-subject GLM maps resulting from step 2.

The nomenclature that we used for the PPC areas is based on recent imaging literature that delineates several large regions tiling the medial SPL using phase-encoding topography (35, 39) and on our own observation of multiple response peaks in the PPC. The first area along the *ips* that showed significant memory-delay activity was V7; more anterior and dorsal was the IPS1. In agreement with previous studies, most significant saccade and memory-delay activation in the posterior (or caudal) *ips* was found medially and in branches extending toward midline. The peak of memory-delay activation was located in a small sulcus running medial and perpendicular to the *ips*, an area that encompassed the IPS2 and retIPS areas. Originally, the "retinotopic" IPS area was defined functionally in a left/right block-design by Medendorp and colleagues (40, 43) as the site with the most pronounced contralateral tuning for memory saccades. The inspection of reported coordinates for various PPC regions from different laboratories suggests that the retIPS area is situated between, and partially overlaps with, IPS2 and IPS3. The putative human "LIP" (the notation is misleading because of its medial branch location) suggested by several studies (37, 44) also overlaps with the IPS2 and retIPS areas. In our dataset, using a similar memory-delay right > left contrast, we did not detect robust bilateral contralateral regions in the PPC in individual subjects. Therefore, in each subject we selected an ROI in the vicinity of reported coordinates for the retIPS area, in the region that showed the highest peak for the contralateral +memory-delay contrast and the peak of the relative contribution map for contralateral cue and memory (Fig. S6*D*); the highest +memory-delay activation peak, regardless of contralaterality, was considered to be IPS2. Usually, a slightly more medial and ventral part of the activation was defined as retIPS, and an adjacent, or overlapping region was defined as IPS2. Even in the group data, the most straightforward cue and memory right > left contrast did not show significant peaks in this area (Fig. S6*C*). Therefore, as in individual datasets, in across-subjects GLM the bilateral retIPS was defined as highest activation for the contralateral +memory-delay contrast overlapping with the contralateral predictor contribution. IPS3 was located more dorsally and anteriorly, and the anterior IPS was located further down the *ips*. On the medial wall of the SPL, the precuneus showed strong and contralateral cue and memory responses.

We emphasize that the exact delineation and terminology of different PPC regions, although important, is not the main focus of the current study and does not affect our principal conclusions. By estimating the response amplitude and contralaterality across several parietal areas involved in the task, both in individual subjects and across subjects, we attempted to present a full

spectrum of task-related responses and to ensure that we did not miss any significant (contralateral) activation.

Human Cortex-Based Alignment. To improve anatomical correspondence beyond Talairach space matching by reducing human intersubject variability of individual gyri/sulci patterns, we also applied cortex-based alignment (45, 46). The gray/white matter boundary of each individual hemisphere was segmented, and the borders of the two resulting segmented subvolumes were tessellated to produce a surface reconstruction. The resulting surface was morphed into a spherical representation, and the hemispheres were aligned based on the curvature information regarding the gyral/sulcal folding pattern. The target of the morphing procedure was a dynamical group average of all included hemispheres. The mapping between the individual hemispheres was used for the realignment of the functional data.

Box S1. ROI definitions

Sulci. [Sulci are written in lower-case italics in the main text and SI text; here, [m], monkey; monkey/human (no superscript); human [h], human]

ps – principal [m]
as – arcuate [m] (*asu* – upper limb; *asl* – lower limb)
cis – cingulate (*acis* – anterior; *pcis* – posterior)
sfs – superior frontal [h]
ifs – inferior frontal [h]
ips – intraparietal
ls – lateral [m]
sts – superior temporal
lus – lunate [m]
pos – parieto-occipital [m]
cas – calcarine
fus – fusiform [h]
tos – transverse occipital [h]
ios – intraoccipital [h]

Other abbreviations. PPC – posterior parietal cortex
SPL – superior parietal lobule (part of PPC)
IPL – inferior parietal lobule (part of PPC)

Monkey brain areas. (Areas are listed in the order used in Table S1.)
Posterior parietal. LIPd/v – lateral intraparietal area, dorsal/ventral (47, 48). Because of its proximity to the border of the axial slice package, the topmost part of *ips* was not consistently activated; thus LIPd refers to the lower part of dorsal division. We further subdivided areas along the *ips* as the anterior LIP (aLIP), and posterior LIP (pLIP; also called "caudal IP," CIP), based on cue and delay responses.

VIP – ventral intraparietal area

LOP – lateral occipital parietal (junction of the *ips* and the *pos,* lateral part)

7a – area 7a in the IPL

Frontal. FEF – frontal eye fields [area 8A, *asu*, and area 45, *asl* dorsal bank; the latter is referred to as the ventral part of FEF, as defined functionally by the microstimulation (49)]. We attempted to distinguish between areas 8A ("FEF" in the text) and area 45 (*cf.* ref. 50).

dlPFC – dorsal lateral prefrontal cortex (area 46, located along the principal sulcus)

SEF – supplementary eye fields (part of the supplementary motor area, SMA, in F3)

a44 – area 44 in ventral premotor area (PMv)

PMd – dorsal (area F2) premotor area; anterior part is in the *asu* (PMd_asu); posterior part is in the arcuate spur (PMd_spur)

8B – area 8B in the *asu*, medial to 8A

preSMA – area F6 (dorsal to the *acis*)

Parieto-temporal in the sts

Tpt – temporo-parietal area (dorsal bank of the *sts,* STG), more anterior and lateral to the TPO.

TPO – temporal parietal occipital area (dorsal bank of the *sts*), also called "superior temporal polysensory area" (STP) (51).

FST – fundus of the *sts*

MT – middle temporal area (posterior/ventral bank of the *sts*)

MSTd/v – middle superior temporal area, dorsal/ventral. The exact partitioning of the MST area currently is not clear (52) and may depend on the functional tests used for parcellation [MSTd and MSTl (1); MSTc and MSTp (53); MSTdp, MSTm, and MSTl (48)]. The MSTd occupies the anterior dorsal bank of the *sts*. The ventral part of MSTv, located in the floor of the *sts*, roughly corresponds to the MSTl of Komatsu and Wurtz (54). We denoted the MSTd/v according to Nelissen et al. (2).

Human brain areas. (Areas are listed in the order used in Table S2; areas marked by * were defined using coordinates reported in corresponding references.)
Posterior parietal. V7* – higher visual occipito-parietal area located in the most posterior *ips* above the junction with the *tos* (35).

IPS1* –*ips* area 1, medial bank (35)

IPS2* – *ips* area 2, medial bank (35)

retIPS* – retinotopic *ips* (40, 43)

IPS3* – *ips* area 3 (39)

pCu – (anterior) precuneus, medial SPL, anterior to the *pos* and posterior to the superior tip of *cis.*

antIPS – anterior *ips*, located near the junction with the postcentral sulcus.

SMG – supramarginal gyrus (IPL)

Frontal. FEF – human FEF complex was located at the intersection of the precentral and the superior frontal sulci and more lateral and inferior along the precentral sulcus. We subdivided it to medial/superior FEF (mFEF) and lateral/inferior FEF (lFEF).

SEF – human SEF/SMA, located on the medial wall of the frontal gyrus

pIFG – posterior inferior frontal gyrus

dlPFC – located in *ifs (*inferior frontal sulcus), middle frontal sulcus and middle frontal gyrus

Temporal-parietal and V5/MT. *asts* – anterior locus around origin of posterior ascending segment of superior temporal sulcus (*sts*) and posterior portion of superior temporal gyrus (STG)

psts – posterior locus in posterior segment *of sts* and middle temporal gyrus (MTG)

MT* – putative V5/MT+ complex (55–57)

1. Komatsu H, Wurtz RH (1988) Relation of cortical areas MT and MST to pursuit eye movements. I. Localization and visual properties of neurons. *J Neurophysiol* 60: 580–603.
2. Nelissen K, Vanduffel W, Orban GA (2006) Charting the lower superior temporal region, a new motion-sensitive region in monkey superior temporal sulcus. *J Neurosci* 26:5929–5947.
3. Tanaka K, Saito H (1989) Analysis of motion of the visual field by direction, expansion/contraction, and rotation cells clustered in the dorsal part of the medial superior temporal area of the macaque monkey. *J Neurophysiol* 62:626–641.
4. Logan DJ, Duffy CJ (2006) Cortical area MSTd combines visual cues to represent 3-D self-movement. *Cereb Cortex* 16:1494–1507.
5. Brown MRG, et al. (2004) Comparison of memory- and visually guided saccades using event-related fMRI. *J Neurophysiol* 91:873–889.
6. Srimal R, Curtis CE (2008) Persistent neural activity during the maintenance of spatial position in working memory. *Neuroimage* 39:455–468.
7. Kastner S, et al. (2007) Topographic maps in human frontal cortex revealed in memory-guided saccade and spatial working-memory tasks. *J Neurophysiol* 97:3494–3507.

8. Mort DJ, et al. (2003) Differential cortical activation during voluntary and reflexive saccades in man. *Neuroimage* 18:231–246.
9. Ettinger U, et al. (2008) Decomposing the neural correlates of antisaccade eye movements using event-related FMRI. *Cereb Cortex* 18:1148–1159.
10. Corbetta M, Kincade MJ, Lewis C, Snyder AZ, Sapir A (2005) Neural basis and recovery of spatial attention deficits in spatial neglect. *Nat Neurosci* 8:1603–1610.
11. Perry RJ, Zeki S (2000) The neurology of saccades and covert shifts in spatial attention: An event-related fMRI study. *Brain* 123:2273–2288.
12. Mort DJ, et al. (2003) The anatomy of visual neglect. *Brain* 126:1986–1997.
13. Himmelbach M, Erb M, Karnath HO (2006) Exploring the visual world: The neural substrate of spatial orienting. *Neuroimage* 32:1747–1759.
14. Dubowitz DJ, et al. (1998) Functional magnetic resonance imaging in macaque cortex. *Neuroreport* 9:2213–2218.
15. Dubowitz DJ, et al. (2001) Direct comparison of visual cortex activation in human and non-human primates using functional magnetic resonance imaging. *J Neurosci Methods* 107:71–80.
16. Durand JB, et al. (2007) Anterior regions of monkey parietal cortex process visual 3D shape. *Neuron* 55:493–505.
17. Orban GA, et al. (2006) Mapping the parietal cortex of human and non-human primates. *Neuropsychologia* 44:2647–2667.
18. Pinsk MA, DeSimone K, Moore T, Gross CG, Kastner S (2005) Representations of faces and body parts in macaque temporal cortex: A functional MRI study. *Proc Natl Acad Sci USA* 102:6996–7001.
19. Sawamura H, Georgieva S, Vogels R, Vanduffel W, Orban GA (2005) Using functional magnetic resonance imaging to assess adaptation and size invariance of shape processing by humans and monkeys. *J Neurosci* 25:4294–4306.
20. Tsao DY, Freiwald WA, Tootell RB, Livingstone MS (2006) A cortical region consisting entirely of face-selective cells. *Science* 311:670–674.
21. Tsao DY, Moeller S, Freiwald WA (2008) Comparing face patch systems in macaques and humans. *Proc Natl Acad Sci USA* 105:19514–19519.
22. Tsao DY, et al. (2003) Stereopsis activates V3A and caudal intraparietal areas in macaques and humans. *Neuron* 39:555–568.
23. Vanduffel W, et al. (2002) Extracting 3D from motion: Differences in human and monkey intraparietal cortex. *Science* 298:413–415.
24. Denys K, et al. (2004) The processing of visual shape in the cerebral cortex of human and nonhuman primates: A functional magnetic resonance imaging study. *J Neurosci* 24:2551–2565.
25. Baker JT, Patel GH, Corbetta M, Snyder LH (2006) Distribution of activity across the monkey cerebral cortical surface, thalamus and midbrain during rapid, visually guided saccades. *Cereb Cortex* 16:447–459.
26. Koyama M, et al. (2004) Functional magnetic resonance imaging of macaque monkeys performing visually guided saccade tasks: Comparison of cortical eye fields with humans. *Neuron* 41:795–807.
27. Nakahara K, Hayashi T, Konishi S, Miyashita Y (2002) Functional MRI of macaque monkeys performing a cognitive set-shifting task. *Science* 295:1532–1536.
28. Fuster JM (1990) Inferotemporal units in selective visual attention and short-term memory. *J Neurophysiol* 64:681–697.
29. Quintana J, Yajeya J, Fuster JM (1988) Prefrontal representation of stimulus attributes during delay tasks. I. Unit activity in cross-temporal integration of sensory and sensory-motor information. *Brain Res* 474:211–221.
30. Zhou YD, Fuster JM (1996) Mnemonic neuronal activity in somatosensory cortex. *Proc Natl Acad Sci USA* 93:10533–10537.
31. Funahashi S, Bruce CJ, Goldman-Rakic PS (1989) Mnemonic coding of visual space in the monkey's dorsolateral prefrontal cortex. *J Neurophysiol* 61:331–349.
32. Chafee MV, Goldman-Rakic PS (1998) Matching patterns of activity in primate prefrontal area 8a and parietal area 7ip neurons during a spatial working memory task. *J Neurophysiol* 79:2919–2940.
33. Schluppeck D, Curtis CE, Glimcher PW, Heeger DJ (2006) Sustained activity in topographic areas of human posterior parietal cortex during memory-guided saccades. *J Neurosci* 26:5098–5108.
34. Khonsari RH, et al. (2007) Lateralized parietal activity during decision and preparation of saccades. *Neuroreport* 18:1797–1800.
35. Schluppeck D, Glimcher P, Heeger DJ (2005) Topographic organization for delayed saccades in human posterior parietal cortex. *J Neurophysiol* 94:1372–1384.
36. Jack AI, et al. (2007) Changing human visual field organization from early visual to extra-occipital cortex. *PLoS One* 2:e452.
37. Sereno MI, Pitzalis S, Martinez A (2001) Mapping of contralateral space in retinotopic coordinates by a parietal cortical area in humans. *Science* 294:1350–1354.
38. Silver MA, Ress D, Heeger DJ (2005) Topographic maps of visual spatial attention in human parietal cortex. *J Neurophysiol* 94:1358–1371.
39. Swisher JD, Halko MA, Merabet LB, McMains SA, Somers DC (2007) Visual topography of human intraparietal sulcus. *J Neurosci* 27:5326–5337.
40. Medendorp WP, Goltz HC, Vilis T (2006) Directional selectivity of BOLD activity in human posterior parietal cortex for memory-guided double-step saccades. *J Neurophysiol* 95:1645–1655.
41. Gnadt JW, Bracewell RM, Andersen RA (1991) Sensorimotor transformation during eye movements to remembered visual targets. *Vision Res* 31:693–715.
42. Saleem KS, Logothetis NK (2006) *A Combined MRI and Histology Atlas of the Rhesus Monkey Brain* (Academic Press, London).
43. Medendorp WP, Goltz HC, Vilis T (2005) Remapping the remembered target location for anti-saccades in human posterior parietal cortex. *J Neurophysiol* 94:734–740.
44. Astafiev SV, et al. (2003) Functional organization of human intraparietal and frontal cortex for attending, looking, and pointing. *J Neurosci* 23:4689–4699.
45. Fischl B, Sereno MI, Tootell RBH, Dale AM (1999) High-resolution intersubject averaging and a coordinate system for the cortical surface. *Hum Brain Mapp* 8: 272–284.
46. van Atteveldt N, Formisano E, Goebel R, Blomert L (2004) Integration of letters and speech sounds in the human brain. *Neuron* 43:271–282.
47. Blatt GJ, Andersen RA, Stoner GR (1990) Visual receptive field organization and cortico-cortical connections of the lateral intraparietal area (area LIP) in the macaque. *J Comp Neurol* 299:421–445.
48. Lewis JW, Van Essen DC (2000) Mapping of architectonic subdivisions in the macaque monkey, with emphasis on parieto-occipital cortex. *J Comp Neurol* 428:79–111.
49. Schall JD, Morel A, King DJ, Bullier J (1995) Topography of visual cortex connections with frontal eye field in macaque: Convergence and segregation of processing streams. *J Neurosci* 15:4464–4487.
50. Petrides M, Pandya DN (2002) Comparative cytoarchitectonic analysis of the human and the macaque ventrolateral prefrontal cortex and corticocortical connection patterns in the monkey. *Eur J Neurosci* 16:291–310.
51. Felleman DJ, Van Essen DC (1991) Distributed hierarchical processing in the primate cerebral cortex. *Cereb Cortex* 1:1–47.
52. Van Essen DC (2004) Surface-based approaches to spatial localization and registration in primate cerebral cortex. *Neuroimage* 23:(Suppl1):S97–S107.
53. Boussaoud D, Ungerleider LG, Desimone R (1990) Pathways for motion analysis: Cortical connections of the medial superior temporal and fundus of the superior temporal visual areas in the macaque. *J Comp Neurol* 296:462–495.
54. Tanaka K, Sugita Y, Moriya M, Saito H (1993) Analysis of object motion in the ventral part of the medial superior temporal area of the macaque visual cortex. *J Neurophysiol* 69:128–142.
55. d'Avossa G, et al. (2007) Spatiotopic selectivity of BOLD responses to visual motion in human area MT. *Nat Neurosci* 10:249–255.
56. Dukelow SP, et al. (2001) Distinguishing subregions of the human MT+ complex using visual fields and pursuit eye movements. *J Neurophysiol* 86:1991–2000.
57. Shulman GL, et al. (1999) Areas involved in encoding and applying directional expectations to moving objects. *J Neurosci* 19:9480–9496.
58. Andersen RA, Asanuma C, Essick G, Siegel RM (1990) Corticocortical connections of anatomically and physiologically defined subdivisions within the inferior parietal lobule. *J Comp Neurol* 296:65–113.
59. Barash S, Bracewell RM, Fogassi L, Gnadt JW, Andersen RA (1991) Saccade-related activity in the lateral intraparietal area. I. Temporal properties; comparison with area 7a. *J Neurophysiol* 66:1095–1108.
60. Pfeuffer J, et al. (2007) Functional MR imaging in the awake monkey: Effects of motion on dynamic off-resonance and processing strategies. *Magn Reson Imaging* 25: 869–882.

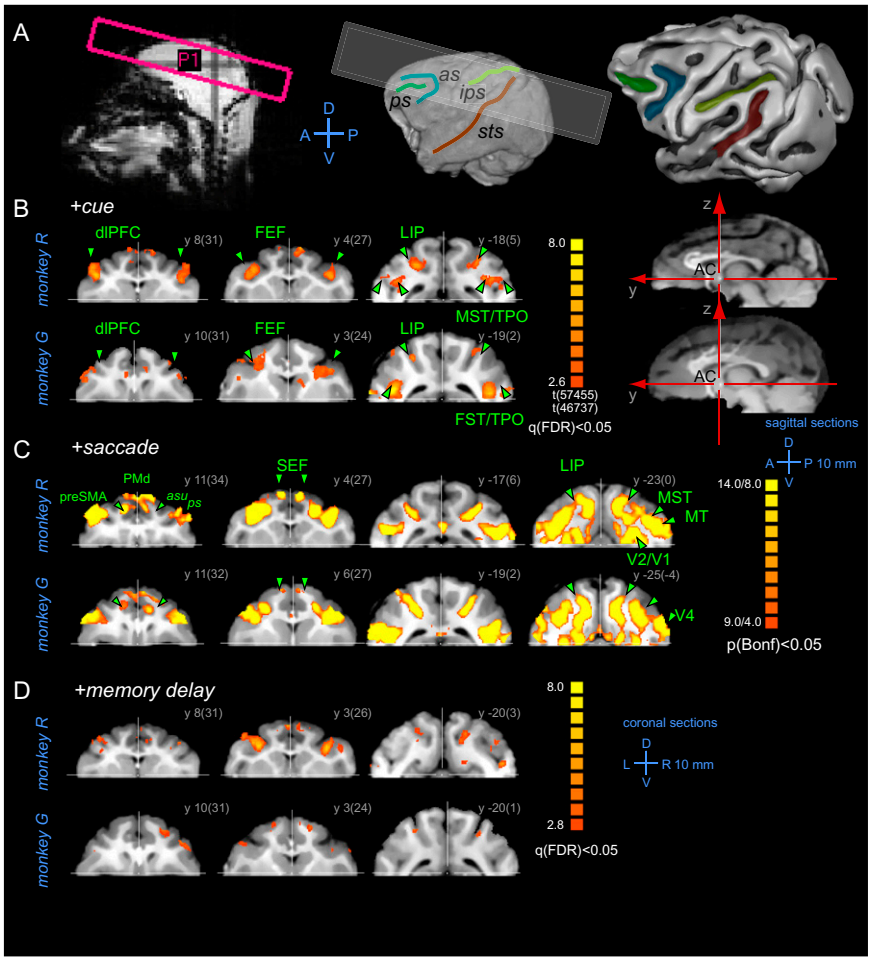

Fig. S1. Activation maps in both monkeys. (*A*) *Left*, Schematic of functional slice package positioning (10 × 2 mm adjacent slices, 15° angle) used in both monkeys, overlaid on the sagittal plane of the pilot localizer scan (P1). *Center*, the same slice package is shown on the 3D reconstruction of the brain surface (monkey G). *Right*, gray-white matter boundary surface (monkey R). Major sulci of interest for this study are depicted: *as*, arcuate; *ips*, intraparietal; *ps*, principle; *sts*, superior temporal. (*B–D*) Cortical areas that were significantly activated using +cue (*B*), +saccade (*C*), and +memory contrasts (*D*), shown in three coronal sections. To demonstrate the consistency between the two monkeys, activation maps are shown separately for each subject. Table S1 summarizes the activation sites. Coronal sections are shown in neurological convention (the left hemisphere is on the left side). In sagittal sections, left corresponds to anterior (A). All monkey brain images are shown in AC–PC bicommissural plane coordinates (AC origin is denoted by the cross-hair; *x*, left–right axis; *y*, posterior–anterior axis; *z*, ventral–dorsal axis). The number next to each slice shows the coordinate of the section relative to the AC origin. The number in parentheses is the position in stereotaxic coordinates, relative to the interaural line. The color bars code significance *t* values; the minimal statistical threshold is shown below. Bonferroni (*P*) or the less conservative false discovery rate *q*(FDR) correction for multiple comparisons was employed.

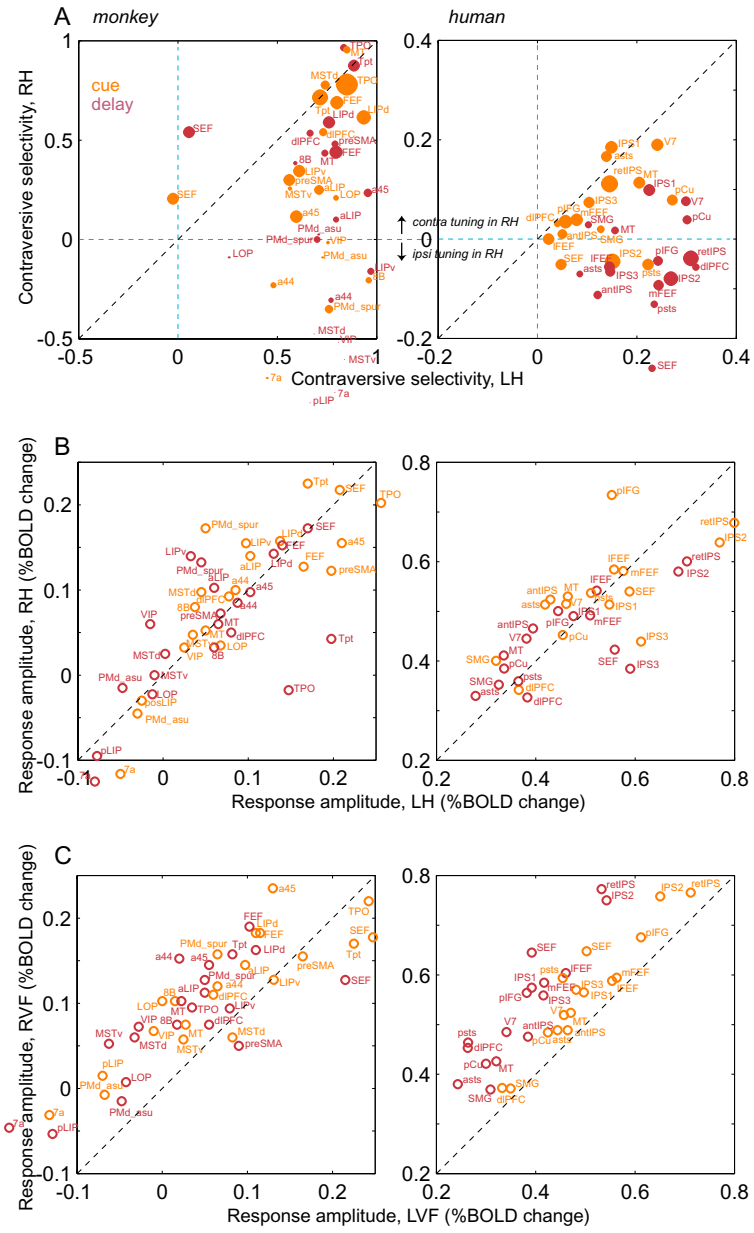

Fig. S2. Hemispheric and visual field asymmetry in monkeys and humans. (*A*) Scatter plots showing right hemisphere (RH) vs. left hemisphere (LH) contraversive selectivity in each area, for cue and memory-delay periods. The size of the dot denotes the mean contralateral response amplitude *A* for each interval. (*B*) Mean cue and delay response amplitude in right vs. left hemisphere. (*C*) Mean cue and delay response amplitude to targets in right vs. left visual field.

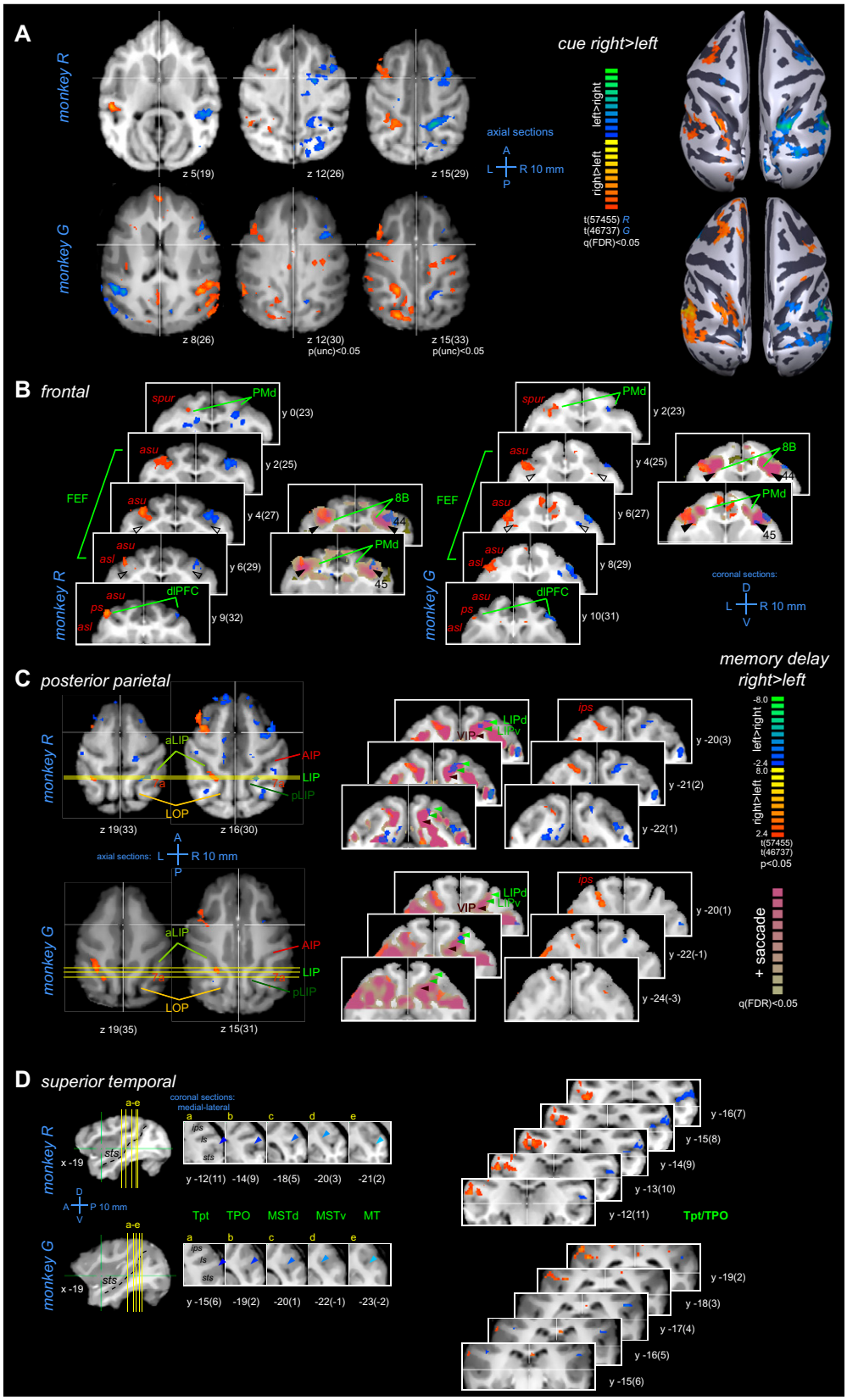

Fig. S3. Maps for the rightward vs. leftward cue and memory-delay contrast in monkeys. (*A*) Cue right vs. left maps are shown on axial slices. Surface reconstructions show the conjunction of +saccade and cue right vs. left contrasts. (*B*) ROIs in the frontal cortex. For each monkey, a sequence of coronal sections going from anterior (*Lower*) to posterior (*Upper*) shows areas that had significant contralateral (memory right vs. left) activation: dlPFC (area 46d/v), FEF (area 8A), and area 45 (in monkey G) and PMd in the arcuate spur (in monkey R). To the right (magenta-brown map, *+saccade* contrast), several sections show areas

Legend continued on following page

that had only cue and saccade activity: areas 44 and 45 in the arcuate sulcus lower limb (*asl*) and area 8B and PMd in the arcuate sulcus upper limb (*asu*). (*C*) ROIs in the PPC. The position of coronal sections across the *ips* portion containing area LIP is shown by yellow lines on axial sections. The most posterior/caudal LIP in the *ips* part parallel to the midline was denoted "pLIP" and may correspond to area CIP or PIP. Note that anterior portion of LIP (aLIP) is distinct from the anterior intraparietal area (AIP), which was not activated in our experiments (*cf.* ref. 1). (*D*) ROIs in the parieto-temporal cortex along the *sts*. The position of coronal sections is shown by yellow lines on the sagittal slice. On the right, right vs. left memory-delay activations in TPO/Tpt are shown. Areas and subdivisions are denoted according to Nelissen et al. (2) and Saleem and Logothetis (3). In monkey G, only a few voxels in the right LIP and TPO/Tpt reached the minimal statistical significance ($P < 0.05$ uncorrected), but the contralateral delay activity in these ROIs was evident in the ERA BOLD time courses.

1. Durand JB, et al. (2007) Anterior regions of monkey parietal cortex process visual 3D shape. *Neuron* 55:493–505.
2. Nelissen K, Vanduffel W, Orban GA (2006) Charting the lower superior temporal region, a new motion-sensitive region in monkey superior temporal sulcus. *J Neurosci* 26:5929–5947.
3. Saleem KS, Logothetis NK (2006) *A Combined MRI and Histology Atlas of the Rhesus Monkey Brain* (Academic Press, London).

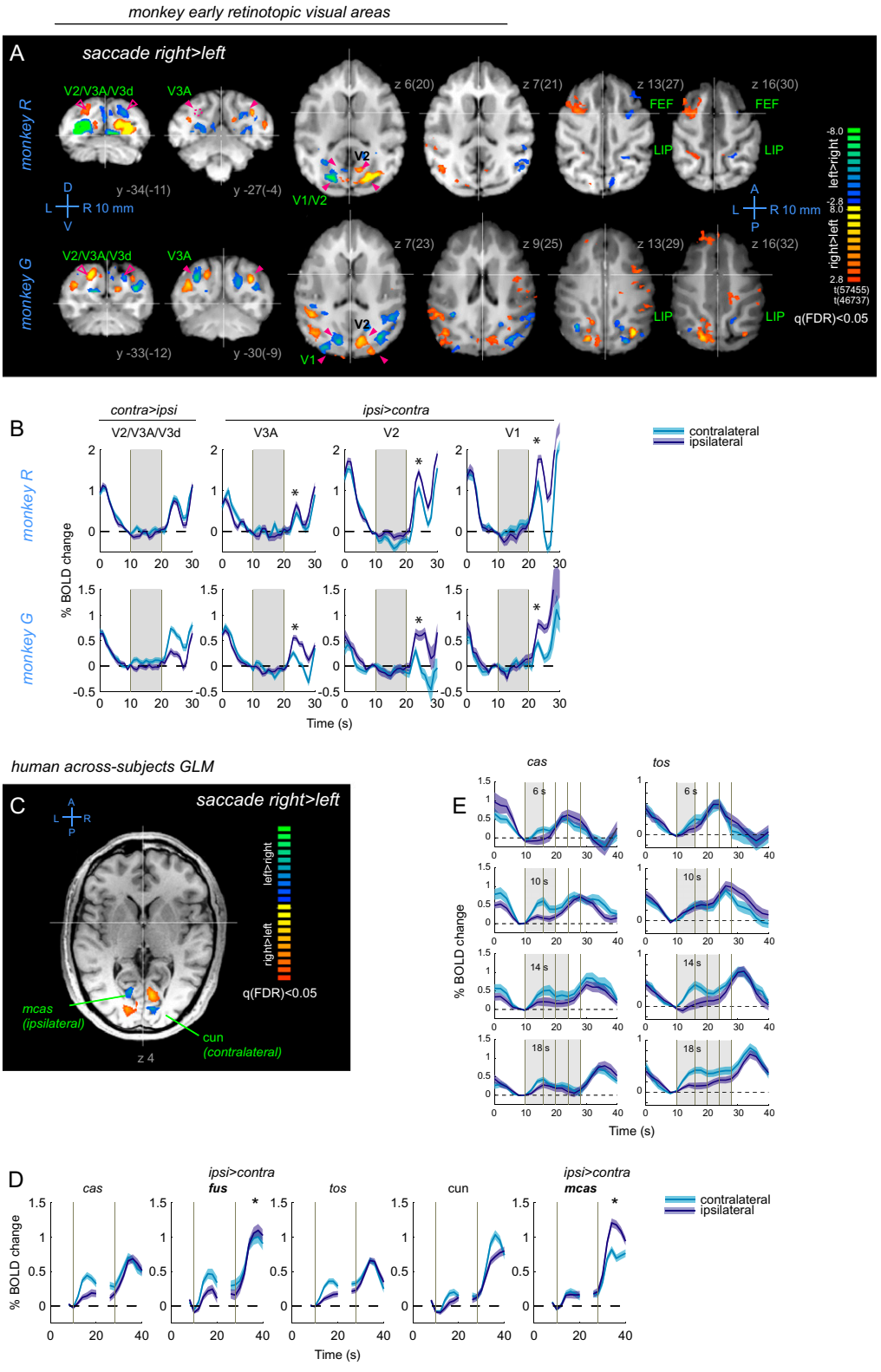

Fig. S4. Contralateral and ipsilateral saccade response tuning in monkeys and humans. (*A* and *B*) In monkeys the frontoparietal and most *sts* areas showed contralateral tuning; the striate and extrastriate early visual areas showed saccadic and postsaccadic (peripheral target hold) tuning for contralateral or ipsilateral saccades, similar to the MSTv area in the *sts* (cf. Fig. S5*C*). (*A*) "Hot" (red-yellow) colors denote positive activation for the rightward > leftward contrast, and "cold" (blue-green) colors indicate positive activation for the leftward > rightward contrast. Images are in neurological convention (the left hemisphere is on the left). In monkey R the activation in the left V3A did not reach statistical significance but was evident with a lowered threshold within the region denoted by the magenta dashed circle. Time-course data from this and other ROIs marked by magenta triangles were used in ERA plots (*B*). Note that in these retinotopic regions the ipsilateral saccade response is larger than the contralateral saccade response (marked by stars in *B*). Ipsilateral tuning could be a result

Legend continued on following page

of peripheral receptive fields moving from a dark area beyond the display to the illuminated background during ipsilateral saccades. Other regions exhibited contralateral tuning (e.g., parafoveal V2/V3A/V3d in the lunate sulcus (*los*), marked by empty triangles), giving rise to a "checkerboard" pattern demonstrating eccentricity tuning shifts between neighboring areas. (*C–E*) In humans, early visual occipital areas showing contra- or ipsilateral tuning for the saccade response. (*C*) Axial slice showing two areas: contralateral-tuned cuneus (cun) and ipsilateral-tuned medial calcarine sulcus (*mcus*). (*D*) ERA time courses from two areas shown in *C* and three more occipital visual areas. Note the weak residual memory-delay activity in the calcarine sulcus (*cas*), fusiform sulcus (*fus*), and transverse occipital sulcus (*tos*) (junction of *tos* and *ios*). (*E*) The residual "memory-delay activity" can be a long carry-over effect of the cue (see *cas*), but sometimes it is present even at the longest 18-s delay (see *tos*), suggesting that it may indeed be present in early occipital areas.

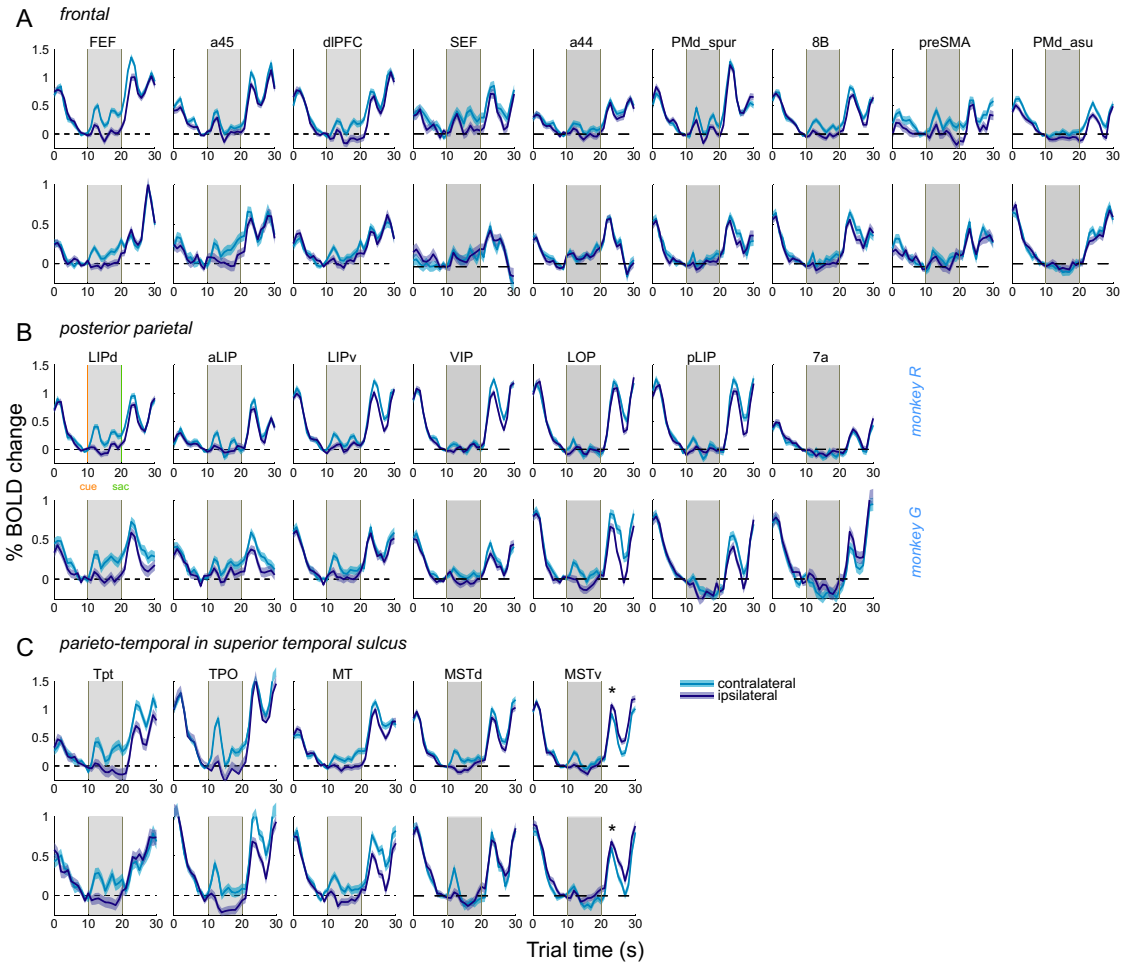

Fig. S5. ERA BOLD trial time courses, shown individually for each monkey. First three columns on the left show areas LIPd/v, aLIP, FEF, dlPFC, MT, TPO, and Tpt that exhibited significant (per sample *t* test, $P < 0.05$) contralateral memory-delay activity in both monkeys (a45 was significant only in monkey G). The rest of cortical areas exhibited little or no memory-delay period activity, or the activity was not consistent in the two monkeys. Conventions are the same as in Fig. 2*C*. (*A*) Frontal ROIs. (*B*) Posterior parietal ROIs. Our functional slice package did not include the topmost part of the parietal lobule, so the uppermost part of dorsal LIP and most of the surface area of 7a were not covered. Regions in area 7a located on the lateral surface of inferior parietal lobule and in the anterior bank of the *sts* exhibited saccade responses and no cue or memory responses, consistent with electrophysiological findings (1, 2). (*C*) Parieto-temporal ROIs in the *sts*. Note the contralateral saccade activation in MSTd and ipsilateral saccade activation in MSTv (*cf.* Fig. S4). In all plots, the trough and subsequent peak after the saccade response correspond to the peripheral target fixation followed by free eye movements during reward expectation, delivery, and the intertrial interval (ITI). Jaw movements and licking during reward cause significant field distortions and affect the shape of BOLD responses (Fig. S7E), but this distortion does not occur until 6 s after the instructed saccade; thus saccade responses were not contaminated by these artifacts.

1. Andersen RA, Asanuma C, Essick G, Siegel RM (1990) Corticocortical connections of anatomically and physiologically defined subdivisions within the inferior parietal lobule. *J Comp Neurol* 296:65–113.
2. Barash S, Bracewell RM, Fogassi L, Gnadt JW, Andersen RA (1991) Saccade-related activity in the lateral intraparietal area. I. Temporal properties; comparison with area 7a. *J Neurophysiol* 66:1095–1108.

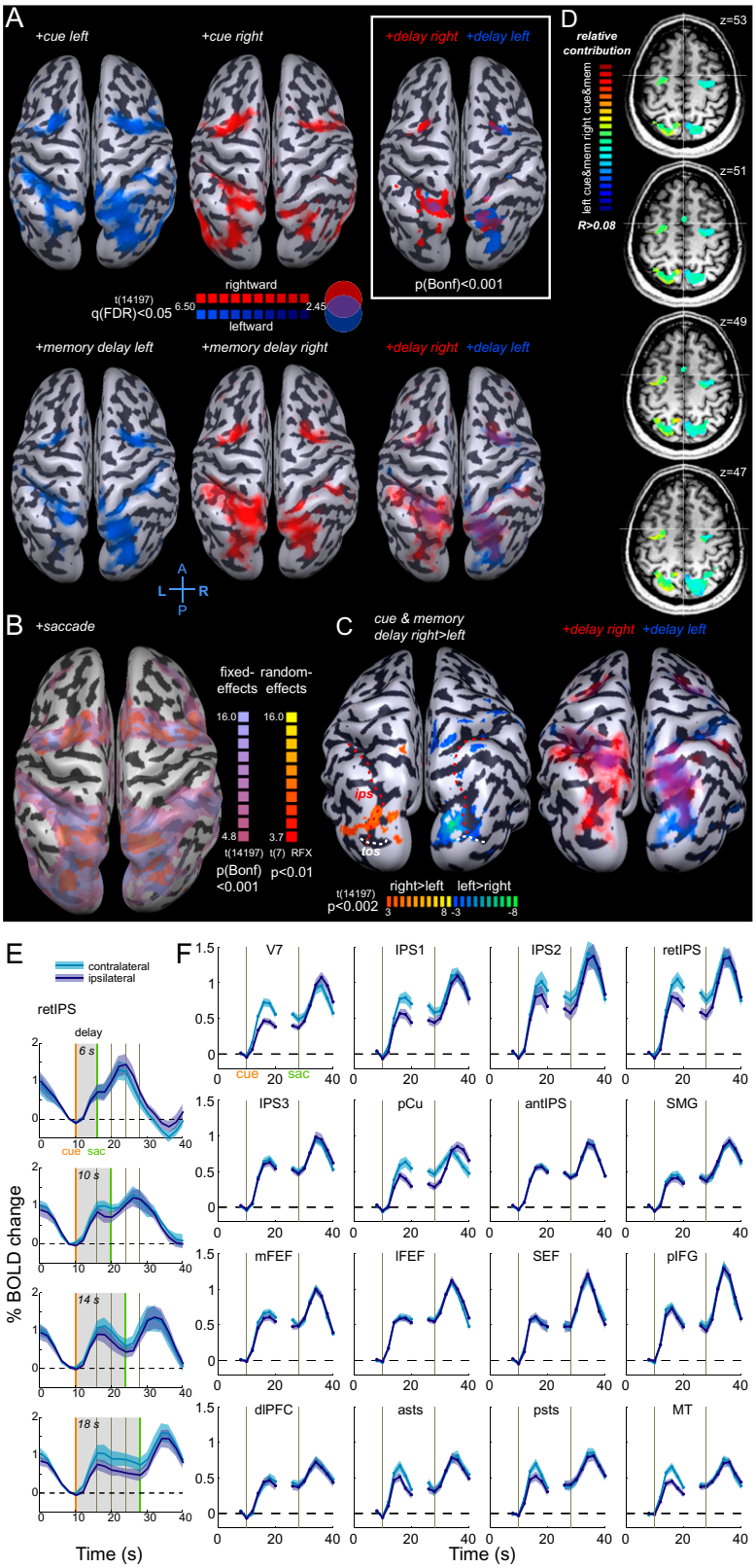

Fig. S6. Human imaging data. Statistical maps for (*A*) +cue left and +cue right contrast (Upper) and +memory left and +memory right contrast (*Lower*). Note stronger and more extensive contralateral activations (except for almost equal left and right memory activation in the right hemisphere). Transparency scales with significance of activation. The combined +memory-delay right and +memory-delay left map is also shown with the higher statistical threshold *P*(Bonf) <0.001, to highlight the peaks of memory-delay activation (white box). (*B*) +saccade (left and right), with the same "random-effects" map superimposed; note the overlap of the two maps in parietal and frontal clusters. (*C*) Cue and memory-delay right > left contrast ($P < 0.002$ uncorrected) shows that significantly

Legend continued on following page

contralateral voxels are localized mostly to the occipital lobe, V7, and precuneus (pCu) but not to areas in the *ips* and FEF with strong delay period activity (*cf.* +memory-delay left and right map). (*D*) Four axial sections showing the relative contribution of left and right cue and memory-delay predictors to variance in significantly activated voxels [*P*(Bonf) <0.001]. Color map ranges from red-yellow (mostly right predictors contribute) to green (equal contribution), to cyan-blue (mostly left). These maps further demonstrate weak but extant contralaterality of human frontoparietal areas. Note a stronger contralaterality in the pCu. (*E*) Sample set of ERA time courses for four delay periods (6, 10, 14, and 18 s) from bilateral ROIs in the retIPS (averaged across eight subjects; shaded areas denote intersubject SEM). (*F*) ERA gap-plots for all delay periods, aligned to cue and to saccade events, in all ROIs.

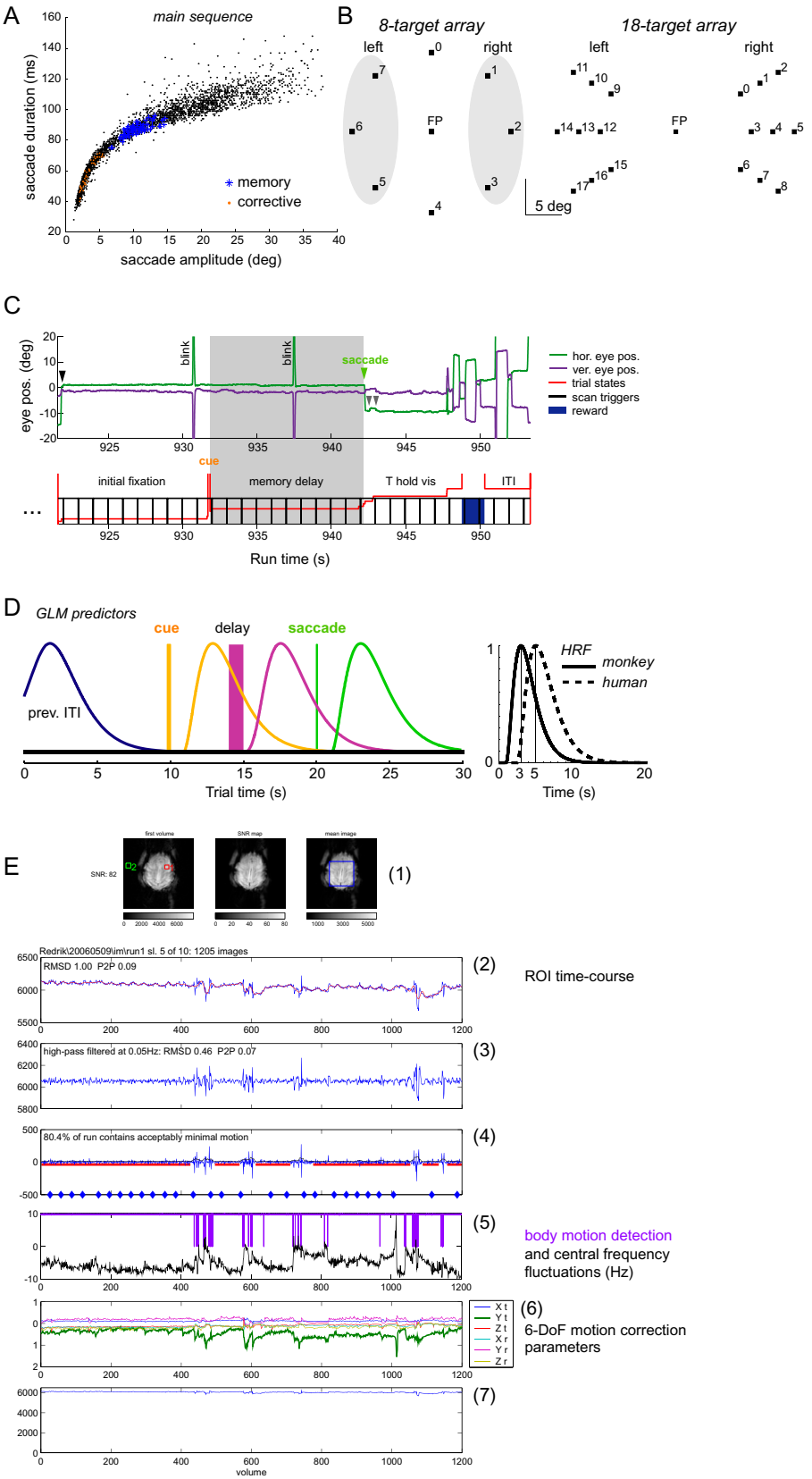

Fig. S7. Methods: eye movement behavior, trial predictors, monkey/human HRF, and data selection. (*A*) Scatter plot of saccadic main sequence (saccade duration vs. saccade amplitude) during one scanning session (monkey G, session 20051030). Instructed memory saccades are denoted by blue stars; corrective saccades that often follow memory saccades are indicated by magenta dots; all other saccades [mostly occurring during the intertrial interval (ITI)] are indicated

Legend continued on following page

by black dots. (*B*) Targets configurations used in the experiments. (*Left*): Eight-target array: targets 1, 2, and 3 were considered "rightward," and targets 5, 6, and 7 were considered "leftward." (*Right*) The18-target left–right array used in a subset of experiments. (*C*) Eye position and trial events in one (memory) trial in a monkey. Saccades are denoted by inverted triangles above the eye-position traces. Lower panel shows trial states, the triggers from scanner (repetition time TR 1 s for each volume), and trigger for the liquid reward dispenser. Because of very long trials (~200/session) and the number of trials was low, each reward was large: ~1 mL (*D*) (*Right*) Trial predictors for the GLM computation in monkeys after convolution with the "monkey HRF." To separate the ensuing memory-delay activity from preceding cue responses, we restricted delay GLM predictors to the second part of the delay period. Different directions were modeled with separate predictors. Only predictors of interest for the current study are shown; we also had predictors for "target hold," "wait for reward," and "reward" epochs. Human predictors had the same structure (except liquid reward) and were convolved with a standard "Boynton" HRF. (*Left*) Single-gamma Boynton HRF function for monkeys: $\delta = 1$, $\tau = 1$, $n = 3$ (solid line) and for humans: $\delta = 2.5$, $\tau = 1.25$, $n = 3$ (dashed line). The monkey HRF rises and returns to the baseline faster than the human HRF (time to peak, 3 and 5 s, respectively) (*cf.* Figs. 2, 4*C*, and 5*A*). Application of the faster HRF for the calculation of predictors in monkeys allowed better capturing of the BOLD response dynamics in GLM. (*E*) Evaluation of EPI SNR, temporal stability. and data selection for event-related analysis. Example of one 20 min run (TR 1 s, 1,200 volumes) in monkey R. (*1*) Single raw EPI slice (first volume), SNR map per voxel (calculated across the run), mean raw EPI image across the run, and ROIs used for SNR calculation (green, background noise; red, signal in arcuate sulcus) and temporal time-course estimation (blue, shown below). (*2*) Raw EPI time course extracted from the large blue ROI (blue curve) and corresponding low-pass filtered signal (cut-off 0.05 Hz; red curve). Two measures of the time-course stability are *root mean square deviation (RMSD)* = $std(ROI_{timecourse})/(mean(ROI_{timecourse})/100)$ and peak-to-peak (P2P) = $(maxROI_{timecourse} - minROI_{timecourse})/minROI_{timecourse}$. (*3*) High-pass filtered signal calculated as original minus low-pass filtered signal. (*4*) The derivative of the high-pass filtered signal, used as an input to an automatic adaptive algorithm that selected epochs unaffected by monkey motion (marked by thick red lines). Blue diamonds denote times of reward delivery. (*5*) Purple curve shows monkey body motion detection signal, black curve represents the fluctuations of the central frequency showing off-resonance changes caused by jaw, head, and body motions (*cf.* ref. 1). Note that body motions and each reward delivery are accompanied by the central frequency changes. (*6*) BrainVoyager 3D motion correction parameters: translation and rotation. Jaw and body motions result in a strong shift in phase-encoding (A-P direction), corresponding to the Y translation (Y_t) (green curve). Note that Y_t curve mirrors the central frequency fluctuation time course. (*7*) Raw-EPI time course replotted on a full scale.

1. Pfeuffer J, et al. (2007) Functional MR imaging in the awake monkey: Effects of motion on dynamic off-resonance and processing strategies. *Magn Reson Imaging* 25:869–882.

Table S1. Monkey data

Cortical area	Left ROI			Right ROI			*CS*			Contrast and minimal *t* value
	x	*y*	*z*	*x*	*y*	*z*	Cue	Delay	Sac	
Posterior parietal areas										
LIPd	−10	−21(2)	19(33)	10	−21(2)	19(33)	0.68	0.89	0.11	3 (2.86)
	−11	−22(-1)	19(37)	12	−22(-1)	17(35)	0.87	0.61	0.12	3 (3.30, $P < 0.001$)
aLIP	−15	−17(6)	16(30)	15	−16(7)	16(30)	0.51	0.39	0.18	2 (2.80)
	−15	−16(5)	17(35)	15	−16(5)	17(35)	0.66	0.84	0.08	2 (3.12)
LIPv	−9	−21(2)	16(30)	9	−21(2)	16(30)	0.63	0.51	0.08	2 (2.8)
	−11	−20(1)	15(33)	11	−22(-1)	15(33)	0.51	0.36	0.08	2 (3.12)
VIP	−8	−20(3)	13(27)	7	−20(3)	13(27)	0.83	0.57	0.15	1 (3.62)
	−8	−20(1)	12(30)	8	−20(1)	13(31)	0.85	−0.10	0.08	1 (3.65)
LOP	−7	−28(-5)	18(32)	9	−27(-4)	18(32)	0.86	0.90	0.11	1 (3.62)
	−9	−30(-9)	18(36)	8	−30(-9)	17(35)	0.29	−0.10	0.04	1 (3.65)
pLIP	−5	−24(-1)	16(30)	5	−24(-1)	16(30)	0.78	−0.72	0.12	1 (3.62)
	−8	−27(-6)	17(35)	7	−27(-6)	16(34)	0.57	0.61	0.08	1 (3.65)
7a	−12	−24(-1)	19(33)	12	−24(-1)	19(33)	−0.51	−0.15	−0.13	1 (3.62)
	−13	−27(-6)	18(36)	13	−27(-6)	17(35)	0.32	−0.23	−0.07	1 (3.65)
Frontal areas										
FEF	−15	4(27)	14(28)	15	3(26)	13(27)	0.78	0.71	−0.06	3 (2.86)
	−15	5(26)	13(31)	17	5(26)	13(31)	0.64	0.81	0.17	2 (3.12)
a45	−16	6(29)	9(23)	16	6(29)	10(24)	0.66	0.76	0.08	2 (2.80)
	−16	6(27)	10(28)	16	6(27)	10(28)	0.27	0.68	0.11	2 (3.12)
dlPFC	−15	9(32)	13(27)	16	9(32)	13(27)	0.82	0.31	0.07	2 (2.80)
	−16	10(31)	13(31)	17	10(31)	13(31)	0.53	0.96	0.14	2 (3.12)
SEF	−4	4(27)	21(35)	5	4(27)	21(35)	0.07	0.00	0.02	1 (3.62)
	−5	6(27)	23(41)	5	6(27)	23(41)	0.12	0.63	0.13	1 (3.65)
a44	−16	4(27)	9(23)	16	3(26)	9(23)	−0.15	0.06	0.02	1 (3.62)
	−14	4(25)	9(27)	14	4(25)	9(27)	0.49	0.90	0.08	1 (3.65)
PMd *spur*	−13	0(23)	17(31)	13	0(23)	16(30)	0.88	0.22	0.06	1 (3.62)
	−13	2(23)	15(33)	12	2(23)	15(33)	0.35	0.70	0.04	1 (3.65)
8B	−12	4(27)	13(27)	13	4(27)	13(27)	0.89	0.33	0.08	1 (3.62)
	−11	4(25)	16(34)	11	4(25)	16(34)	0.68	0.92	0.13	1 (3.65)
preSMA	−3	11(34)	14(28)	4	11(34)	15(29)	0.25	0.24	0.06	1 (3.62)
	−4	11(32)	16(34)	5	11(32)	15(33)	0.45	0.96	0.11	1 (3.65)
PMd *asu*	−10	8(31)	16(30)	10	8(31)	16(30)	−0.44	−0.72	0.13	1 (3.62)
	−10	6(27)	16(34)	11	6(27)	16(34)	0.89	0.76	0.23	1 (3.65)
Parieto-temporal areas in mid-to-posterior superior temporal sulcus										
Tpt	−26	−12(11)	5(19)	26	−13(10)	3(17)	0.89	0.96	−0.08	3 (2.86)
	−26	−16(5)	8(26)	26	−16(5)	8(26)	0.58	0.98	0.21	2 (3.12)
TPO	−24	−14(9)	4(18)	24	−13(10)	4(18)	0.88	0.95	0.16	3 (2.86)
	−23	−19(2)	8(26)	23	−19(2)	9(27)	0.78	0.97	0.05	2 (3.12)
MT	−18	−21(2)	8(22)	18	−21(2)	8(22)	0.96	0.54	0.18	1 (3.62)
	−17	−23(-2)	10(28)	17	−23(-2)	10(28)	0.94	0.79	0.08	2 (3.12)
MSTd	−21	−18(5)	7(21)	−21	−18(5)	6(20)	0.52	−0.15	0.01	1 (3.62)
	−19	−20(1)	10(28)	21	−20(1)	8(26)	0.97	0.29	0.07	2 (3.12)
MSTv	−17	−20(3)	10(24)	16	−21(2)	10(24)	0.10	−0.91	−0.09	1 (3.62)
	−15	−22(-1)	9(27)	15	−22(-1)	9(27)	0.95	0.79	−0.08	1 (3.65)
Early visual areas (special contrast **4:** [saccade right > saccade left, q(FDR)<0.05])										
V1	−8	−36(-13)	6(20)	7	−36(-13)	6(20)	0.83	−0.04	−0.25	4 (3.00)
	−14	−38(-17)	7(25)	11	−40(-19)	7(25)	0.95	0.24	−0.20	4 (2.86)
V2	−5	−29(-6)	7(21)	5	−29(-6)	7(21)	0.79	−0.13	−0.36	4 (3.00)
	−6	−35(-14)	7(25)	5	−35(-14)	7(25)	−0.34	−0.95	−0.16	4 (2.86)
V3A	−12	−25(-3)	13(27)	17	−25(-2)	12(26)	0.80	−0.82	−0.28	4 (3.00)
	−14	−29(-8)	14(32)	14	−29(-8)	12(30)	0.16	0.91	−0.19	4 (2.86)
V3d	−10	−33(-10)	14(28)	10	−33(-10)	14(28)	0.92	0.53	0.41	4 (3.00)
	−8	−32(-11)	16(34)	14	−31(-10)	13(31)	0.92	0.42	0.04	4 (2.86)

First and second columns*:* activated areas and coordinates for left and right ROIs presented in the paper in AC–PC bicommissural space. Stereotaxic coordinates are in parentheses; the angle between the AC–PC plane and the stereotaxic interaural–lower orbital plane was 0° for both monkeys. Third column: individual contraversive selectivity (*CS*) indices. For each entry, the upper row is monkey R, and the lower row is monkey G. Fourth column: statistical contrast used [1, +saccade, q(FDR) < 0.001; 2, +saccade and +cue; 3, +saccade and +cue and +memory delay, q(FDR) < 0.05] and minimal t-value. See also the list of ROI definitions in Box S1.

Table S2. Human data

	Left ROI			Right ROI		
Cortical area	*x*	*y*	*z*	*x*	*y*	*z*
Posterior parietal areas (SPL and IPL)						
V7*	−25	−78	26	24	−78	27
	−25	−77	27	24	−78	27
IPS1*	−20	−70	39	20	−71	37
	−16	−72	40	13	−71	40
IPS2*	−22	−63	50	19	−65	48
	−19	−64	47	20	−68	46
retIPS*	−20	−63	48	18	−64	46
	−20	−62	46	20	−64	46
IPS3*	−25	−53	52	25	−56	52
	−25	−54	50	22	−55	50
pCu	−6	−48	49	4	−50	49
	−4	−49	47	7	−50	47
antIPS	−33	−45	46	31	−48	47
	−35	−38	41	35	−43	45
SMG (IPL)	−54	−32	32	54	−34	32
	−52	−35	32	55	−39	28
Frfontal areas						
mFEF	−22	−6	52	22	−8	57
	−21	−5	58	24	−8	58
lFEF	−35	−10	50	36	−8	52
	−32	−8	47	28	−8	50
SEF	−4	3	52	5	6	51
	−3	8	50	4	7	50
pIFG	−46	0	34	46	3	35
	−45	0	31	41	−1	40
dlPFC	−32	34	32	31	37	34
	-37	*27*	*31*	*35*	*30*	*31*
Parieto-temporal areas and V5/MT complex						
asts	−52	−44	11	50	−40	14
	−47	−41	12	45	−43	12
psts	−48	−56	7	44	−50	5
	−47	−56	7	45	−45	7
V5/MT*	−45	−61	5	40	−61	7
	−45	−61	6	45	−60	5
Occipital early visual areas (extracted from across-subjects GLM only)						
cas	−29	−60	−5	25	−61	−9
fus	−25	−67	−16	19	−67	−16
tos	−27	−76	9	28	−76	8
cun	−11	−85	−1	10	−84	4
mcas	−14	−68	3	9	−70	2

Activated areas and Talairach coordinates for ROIs presented in the paper. For each entry, the upper row gives the average of values derived from individual-subject GLMs, and the lower row gives across-subjects GLM. Anatomy definitions are based on ref. 1.

*Areas were defined using coordinates reported in the literature (see list of ROI definitions in Box S1).

1. Duvernoy, et al. (1999) The human brain: Surface, three-dimensional sectional anatomy with MRI, and blood supply (Springer, New York).